JOURNAL OF MATERIALS SCIENCE 33 (1998) 515–522

Hexavalent chromium in tricalcium silicate

Part II *Effects of Cr^{VI} on the hydration of tricalcium silicate*

O. E. OMOTOSO, D. G. IVEY
Department of Mining, Metallurgical and Petroleum Engineering, University of Alberta, Edmonton, Canada T6G 2G6

R. MIKULA
CANMET Western Research Centre, Devon, Alberta, Canada TOC 1E0

The composition and structure of hydrated tricalcium silicate (C_3S)* pastes admixed with Cr^{VI} have been studied. The resultant mixture simulates Cr^{VI} waste forms stabilized in ordinary Portland cement. Scanning electron microscopy and transmission electron microscopy were used to identify the microstructural changes accompanying the addition of Cr^{VI} solutions to C_3S. Energy-dispersive X-ray spectroscopy was used to probe the distribution of chromium in the phases within the hazardous waste forms. Elucidation of the molecular structure of the reaction products was accomplished with Fourier transform infrared and nuclear magnetic resonance spectroscopies.

Cr^{VI} was found to be contained in the waste form as soluble $Ca_2CrO_5 \cdot 3H_2O$ and partially chemically bonded within the calcium silicate hydrate (C–S–H) phase. Cr^{VI} was also found to increase the condensation of C–S–H and porosity of the waste form.

1. Introduction

Calcium silicate hydrate (C–S–H) is the main hydration product of tricalcium silicate (C_3S). It is amorphous, has a variable composition and can assume different morphologies. C–S–H is broadly classified into early and late C–S–H [1]. "Early C–S–H", which contains dimeric silicate units, appears as fibres or foils and starts to form after about 6 h from the onset of reaction. A more condensed "late C–S–H" starts to form after about 1 day. It contains polymeric silicate units. A completely hydrated paste contains calcium hydroxide (CH) and $CaCO_3$ in addition to C–S–H.

Much work has been done to elucidate the modifying effects of admixtures on the setting and hardening of cement. These studies serve as a reference for understanding the containment mechanisms of hazardous wastes in cement. Kantro [2] investigated the hydration of C_3S in the presence of various salts. He observed that most soluble salts accelerate the hydration of C_3S, notable exceptions being phosphates, fluorides and salts of Zn, Sn and Pb. His data suggest that both the charge and the atomic size of the ions are important. Those with high charge and small size are the most effective accelerators. The approximate order of effectiveness is as follows [3]:

$$Y^{3+} \approx La^{3+} \approx Ca^{2+} > Ni^{2+} > Mg^{2+} > Sr^{2+}$$

$$> Ba^{2+} \approx Li^{+} > K^{+} > Rb^{+} \approx Cs^{+} > Na^{+}$$

for chlorides, and

$$Cl^- > S_2O_3^{2-} > Br^- > NO_2^- > CrO_4^{2-} > NO_3^-$$

$$> SCN^- > I^- > ClO_4^- > SO_4^{2-}$$

for calcium salts [4].

In a review by Thomas [4], it was reported that anions of soluble salts give rise to a porous C–S–H because of their high deflocculating power. Depending on their mobilities, the anions easily pass through the permeable C–S–H membrane, increasing the osmotic pressure and causing the membrane to rupture faster than would occur if the pure solution contained only water. The resultant rupture exposes the anhydrous C_3S to further rapid reaction. The chemistry of Cr^{VI} is essentially that of its anion (CrO_4^{2-}). Microstructural studies of Cr^{VI}-doped C_3S indicate that the porosity of hydrated paste is high [5]. Hydration retarders permit the precipitation of a dense C–S–H. The induction period is extended [4, 6], reducing the permeability and thus the passage of ions.

Several methods have been used to determine the composition of C_3S pastes. Methods for determining the amount of CH include thermogravimetry, differential thermal analysis, quantitative X-ray diffraction (QXRD), back-scattered electron image analysis and solvent extraction [7–10]. QXRD and ^{29}Si solid-state nuclear magnetic resonance (NMR) can be used to determine the amount of unreacted C_3S in partially hydrated pastes, with a precision of no better than 3%

* The cement notation used throughout is: C = CaO; S = SiO_2; H = H_2O; CH = $Ca(OH)_2$; C_3S = Ca_3SiO_5; C–S–H = calcium silicate hydrate.

0022–2461

[1]. Generally, a fully hydrated C_3S paste contains about 35% CH, some of which would be carbonated to $CaCO_3$ depending on the hydrating environment. If the amounts of CH and CO_2 in a fully hydrated paste are known, the Ca-to-Si ratio in the C–S–H can be determined. The Ca-to-Si ratio calculated using extraction and thermal methods is 1.7 ± 0.1 and 1.99 for QXRD [1, 8].

Electron microscopy coupled with X-ray microanalysis has been extensively used to investigate the structural, morphological and chemical development of the different types of C–S–H. Scanning electron microscopy (SEM) is particularly convenient for analysing fracture surfaces without difficult sample preparation [11–18]. Back-scattered electron imaging of polished surfaces can provide information about the compositional variations in dense regions which would not be otherwise observed with secondary-electron imaging of fracture surfaces. Transmission electron microscopy (TEM) has the greatest potential for high spatial resolution [16, 19–24]. The difficulties involved in preparing thin samples is reduced by dimpling 3 mm discs, followed by ion milling of liquid-nitrogen-cooled specimens for about 3 h to produce relatively large thin sections suitable for TEM analysis [25].

X-ray microanalysis of polished surfaces has shown the measured Ca-to-Si ratio of C–S–H to be dependent on the accelerating voltage. The ratio can range from 1.4 at 6 kV to 2.0 at 25 kV [26]. Mean values of 1.72 and 1.78 were obtained when operating at 10 kV with a range between 1.5 and 2.0. X-ray microanalysis in the transmission electron microscope indicates a wider range of Ca-to-Si ratios, namely 1.2–2.0 with a mean of 1.4 [27, 28], and no significant difference was found between the Ca-to-Si ratios of inner and outer C–S–H.

The condensation of the silicate and aluminate units, as well as the presence of hydroxyl groups in CH and hydrated calcium chromates, can be followed using infrared spectroscopy. Many of the characteristic vibrations are specific, enabling unambiguous assignments to different structural units in a unit cell. Polymerization of the silicate units in C–S–H results in a reduction of the Si–O–Si bond length to about 0.160 nm from about 0.167 nm [29, 30]. An attendant increase in the force constant causes the asymmetric stretching vibration shifts to higher wave numbers [31–33].

Trimethylsilylation and solid-state ^{29}Si magic angle spinning (MAS) NMR have been used to study the silicate structure of C–S–H during the course of cement hydration [34–43]. In the trimethylsilylation method, the silicate is converted into the corresponding silicic acid with the replacement of SiOH with $SiOSi(CH_3)_3$. In this form, the monomer, dimer and individual polysilicate ions can be separated. The resulting derivatives are analysed using gas–liquid chromatography or gel permeation chromatography [1]. ^{29}Si MAS NMR complements trimethylsilylation and does away with the side effects associated with the chemical procedure of trimethylsilylation. However, it cannot identify individual polysilicate ions, while silylation potentially can [44]. The chemical shifts of the resonances of the ^{29}Si nuclei in silicates are dependent on the degree of condensation of the silicate tetrahedra and on the nature of the X group in Si–O–X (where X can be metallic cations present in the cement matrix). Increasing diamagnetic shielding of the ^{29}Si nucleus with increasing condensation leads to higher-field chemical shifts. Resonances can therefore be assigned to ^{29}Si nuclei in units of a particular condensation as follows: orthosilicate units, SiO_4^{4-} (Q_0); terminal units, $Si(OSi)O_3^{3-}$ (Q_1); internal units, $Si(OSi)_2O_2^{2-}$ (Q_2); branching units, $Si(OSi)_3O^-$ (Q_3); cross-linking units, $Si(OSi)_4$ (Q_4) [45]. The subscripts denote the number of SiO_4^{4-} tetrahedra attached to the main orthosilicate unit. The outer fibrous C–S–H is a dimer (Q_1) while the inner C–S–H that forms late is a polymer with Q_2 units. Since the NMR signal intensity is proportional to the number of nuclei present, the extent of the reaction can easily be followed. The use of MAS NMR with cross-polarization results in a distinction between silicate tetrahedra bonded to hydrogen and those that are not. This has permitted investigators [36, 40], to distinguish between monomeric C–S–H and unreacted C_3S (both are composed of the orthosilicate anion Q_0).

This study is focused on better understanding the nature of C–S–H in the presence of Cr^{VI} from early to late stages of hydration. This is essential in view of the fact that C–S–H is responsible for the strength and stability of monolithic waste forms stabilized in ordinary Portland cement (OPC). Electron microscopy techniques, as well as Fourier transform infrared (FTIR) and NMR spectroscopies, are used to characterize the hydration reactions of chromium-doped C_3S.

2. Materials and methods

The sample preparation methods have been described elsewhere [46]. CrO_3 solutions containing 0.1 mol dm^{-3}, 1 mol dm^{-3} and 2 mol dm^{-3} concentrations were mixed with C_3S in a C_3S-to-solution ratio of about 0.5. The hydration reaction was stopped after 5 min, 6 h, 1 day, 3 days and 60 days.

2.1. Scanning electron microscopy

A Hitachi S-2700 scanning electron microscope equipped with a Link eXL energy-dispersive spectrometer was used for microstructural and microanalytical characterization of the hydrated samples. Polished and fracture sections were characterized. Because of the high porosity of the pastes, polished sections were usually impregnated with a low-viscosity epoxy prior to grinding and polishing [47]. Otherwise the pores may entrap grinding and polishing abrasives. It is important to use oil as water will react with unhydrated C_3S or dissolve soluble components especially in the Cr^{VI}-doped samples. The use of SiC is also discouraged since some pores will escape impregnation and entrap SiC. Energy-dispersive X-ray spectroscopy (EDS) analysis of the regions affected will be misleading as Si is present in many of the phases of interest. Polished and fractured sections were carbon coated prior to analysis.

An accelerating voltage of 20 kV was used for imaging and microanalysis. X-ray data were acquired

for 100 s life time at greater than 2500 counts s^{-1}. Unreacted C_3S in the hydrating pastes and $CaCrO_4 \cdot 2H_2O$ were used as standards to calculate the Ca-to-Si and the Ca-to-Cr ratios in the C–S–H and calcium chromate phases.

2.2. Transmission electron microscopy

Characterization by TEM was done on a JEOL 2010 transmission electron microscope equipped with a Noran Ge energy-dispersive detector. The method described by Ivey and Neuwirth [25] was used for the preparation of thin sections. Samples were carbon coated prior to characterization by TEM.

The probe size used for compositional analysis was about 10 nm and data were collected for 100 s live time. Quantification is simpler than by SEM since, for a thin specimen, absorption and fluorescence effects are negligible. The weight ratio of two elements will then be proportional to their X-ray intensities [48]:

$$\frac{C_A}{C_B} = k_{A/B}\frac{I_A}{I_B} \quad (1)$$

where C_A and C_B are the concentrations in weight per cent of elements A and B, respectively, I_A and I_B are the corresponding X-ray intensities and $k_{A/B}$ is the Cliff–Lorimer factor. The k factors were determined by analysing areas containing unhydrated C_3S and $CaCrO_4 \cdot 2H_2O$.

2.3. Fourier transform infrared spectroscopy

Powdered samples, less than 5 μm in size, were used for FTIR spectroscopy. The classical disc technique was used with caesium iodide pellets to prepare FTIR samples. The spectra were collected on a Nicolet 750 Magna spectrometer between 450 and 4000 cm^{-1}.

2.4. Nuclear magnetic resonance

Powdered samples were also used for ^{29}Si solid-state MAS NMR. The high-resolution solid-state NMR spectra were recorded at 59.63 MHz on a Bruker M SL-300 spectrometer. Samples were spun at 4.5 kHz at the magic angle to the external field. A relaxation delay of 10 s was used for all the samples. About 5000 scans were usually collected. This yielded a satisfactory signal-to-noise ratio in most cases. Q_8M_8 (trimethylsilyl ester of the four ring octameric silicate) was used as the secondary standard. Its major ^{29}Si chemical shift was assigned as $+11.5$ p.p.m. down-field from tetramethysilane. Identification of the different silicate polyhedra was made based on the work of Lipmma *et al.* [34, 35].

Ratios of the Q_1 (dimer) to Q_2 (polymer) were obtained by fitting a Voigt function to the peaks and integrating.

3. Results and discussion

3.1. Electron microscopy

The fibrous morphology assumed by the early C–S–H is shown in the scanning electron micrograph of a 1-day-old blank paste (Fig. 1). Fig. 2a shows

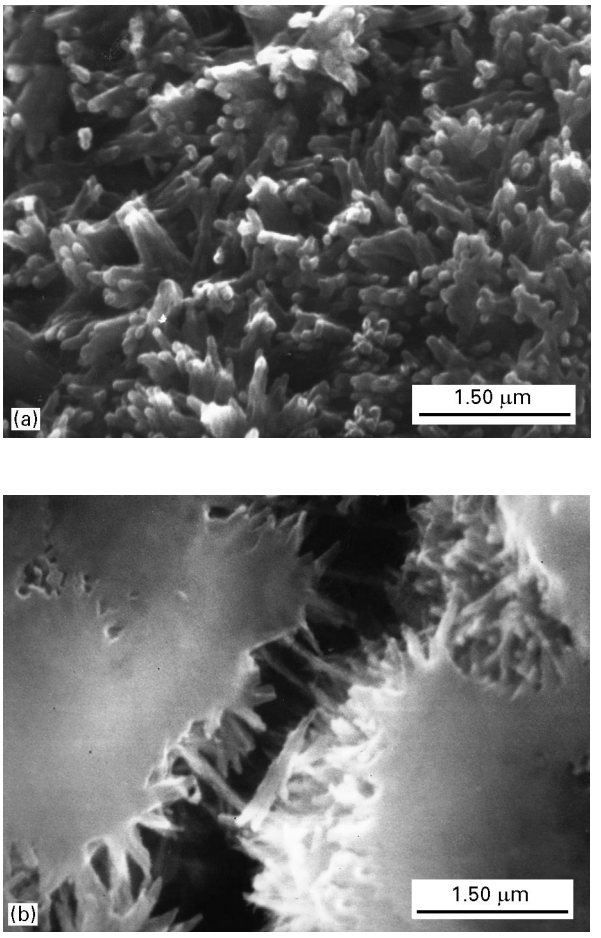

Figure 1 Scanning electron micrographs of a 1-day-old blank paste showing fibrous C–S–H: (a) fracture surface; (b) polished surface.

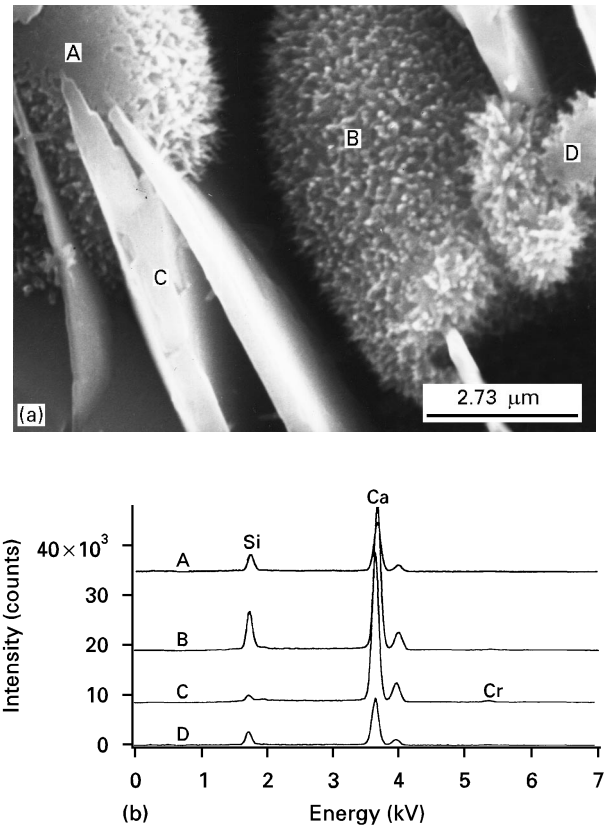

Figure 2 (a) Scanning electron micrograph and (b) EDS spectra of a typical 0.1 mol $Cr^{VI}\,dm^{-3}$ paste hydrated for 1 day. The analysed regions are mainly CH and C–S–H.

a scanning electron micrograph of a 1-day-old 0.1 mol $Cr^{VI}dm^{-3}$ paste. Cr was found to be associated with both CH and fibrous C–S–H as shown in energy-dispersive X-ray spectra in Fig. 2b. The distinct nature of the hydration products without the connectivities observed in the corresponding blank was striking. This suggested a highly porous structure. The C–S–H fibres could be seen to be shorter than the fibrous C–S–H in the blank paste. The approximate Ca-to-Si ratio of the C–S–H gel was found to be 1.8 ± 0.1. In the blank paste, a volume increase is associated with the growth of C–S–H such that, after 60 days, a dense microstructure comprising C–S–H and CH dominate the fracture surfaces (Fig. 3a). This porous structure in 0.1 mol $Cr^{VI}dm^{-3}$ paste persisted in the 60-day-old samples, as depicted in Fig. 3b. The only difference between the 1-day-old and 60-day-old pastes was the greater amount of CH seen in the microstructure of the 60-day-old paste. The average Ca-to-Si ratio of the fibrous C–S–H was essentially the same as for the blank paste, i.e., 1.8 ± 0.1. In analysing these fracture surfaces, care was taken to focus the beam on relatively flat surfaces to reduce the generation of secondary X-rays from surrounding structures.

Doping C_3S with a 1 mol $Cr^{VI}dm^{-3}$ solution gave microstructures similar to the 0.1 mol $Cr^{VI}dm^{-3}$. Shown in Fig. 4a is a scanning electron micrograph of a fractured 60-day-old paste, which is similar to the 1-day-old 0.1 mol $Cr^{VI}dm^{-3}$ pastes. The microstructure remained porous with CH and C–S–H dominating the structure. Microanalysis of the 60-day-old polished sections revealed a phase containing only Ca and Cr with no Si. Fig. 4b shows an X-ray map of the polished section. The phase in the top left corner of the micrograph could be seen to contain only Ca and Cr. X-ray microanalysis indicated that the Ca-to-Cr ratio was 2.1 ± 0.1. This is in agreement with a $Ca_2CrO_5 \cdot 3H_2O$ identified from X-ray diffraction studies [46].

Shown in Fig. 5a is a scanning electron micrograph of a 2 mol $Cr^{VI}dm^{-3}$ paste hydrated for 5 min. The large crystals are $CaCrO_4 \cdot 2H_2O$, which were confirmed by detailed X-ray microanalysis in the transmission electron microscope. Fig. 5b shows a transmission electron micrograph of a calcium chromate phase. The Ca-to-Cr mole ratio was found to be 1.0 ± 0.1. Some C–S–H-containing Cr was also observed in the 5-min-old thin section. The Ca-to-Si ratio was found to be 1.7 ± 0.4. Fig. 5c depicts the compositional relationships in the phases analysed.

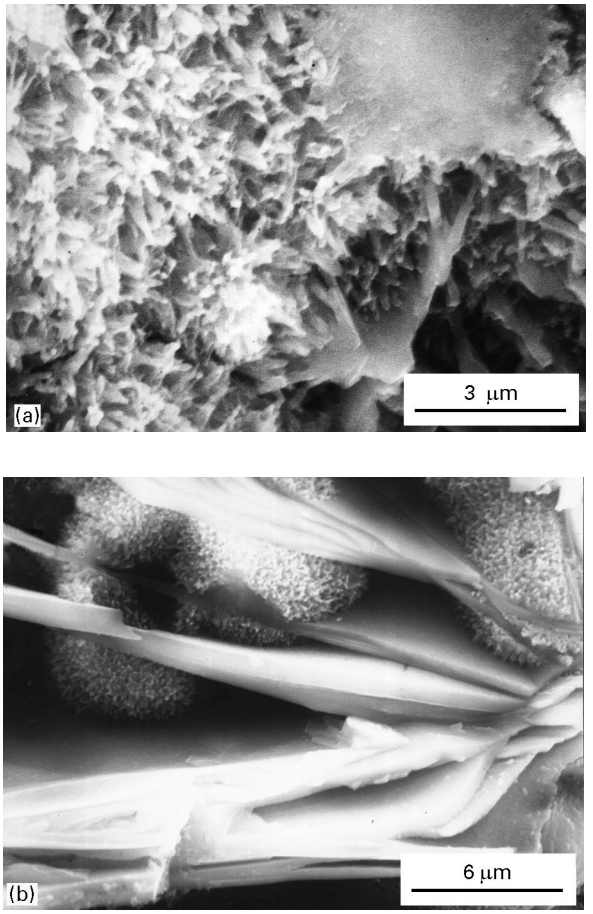

Figure 3 Scanning electron micrograph of 60-day-old pastes: (a) blank paste showing fibrous C–S–H and CH; (b) 0.1 mol $Cr^{VI}dm^{-3}$ paste. Long CH crystals and fibrous C–S–H dominate the structure.

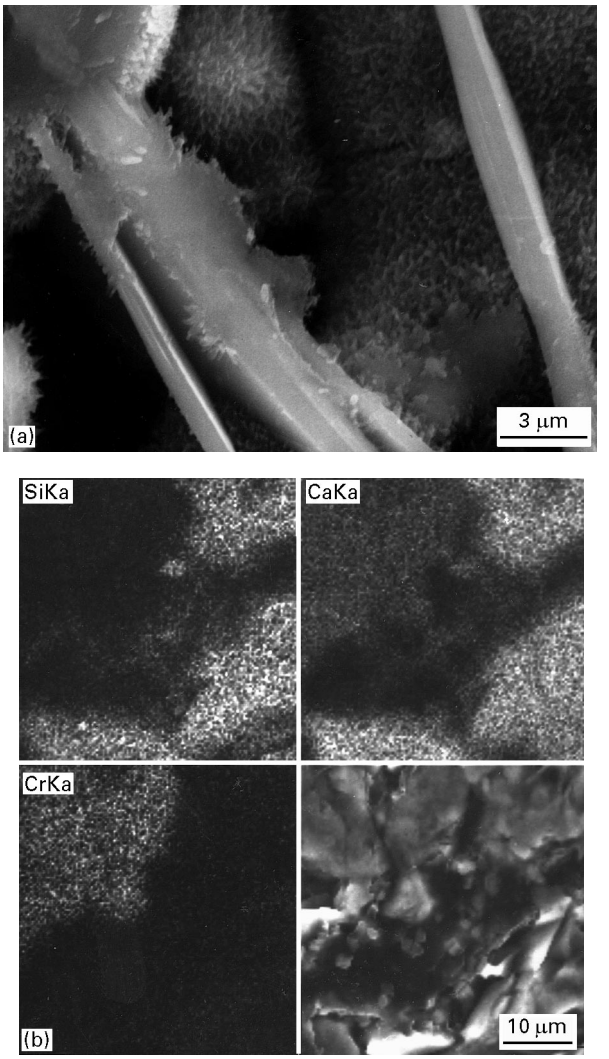

Figure 4 (a) Scanning electron micrograph of 1 mol $Cr^{VI}dm^{-3}$ paste hydrated for 60 days; (b) X-ray map of a polished 1 mol $Cr^{VI}dm^{-3}$ paste hydrated for 60 days, showing the distribution of Ca, Si and Cr in the reaction products.

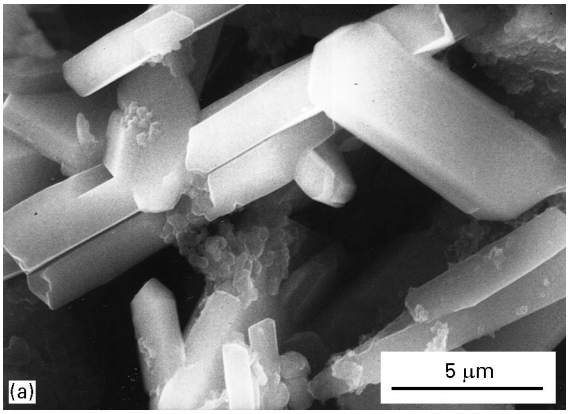

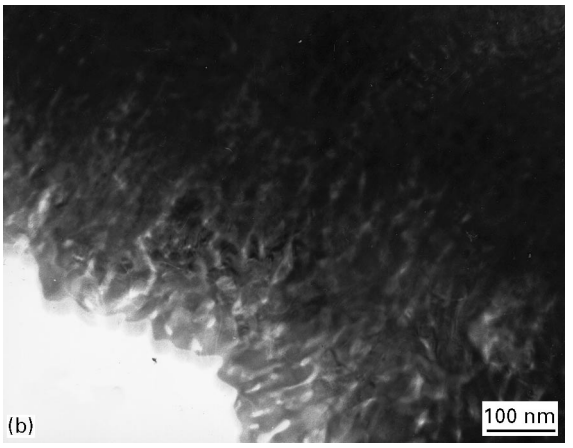

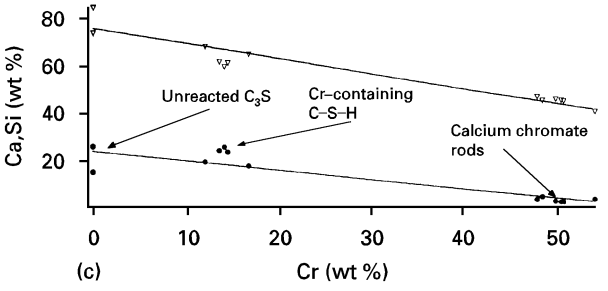

Figure 5 (a) Scanning electron micrograph of a 5-min-old 2 mol $Cr^{VI}dm^{-3}$ paste; (b) transmission electron micrograph of the $CaCrO_4 \cdot 2H_2O$ phase; (c) TEM/X-ray microanalysis of typical phases in a 5-min-old 2 mol $Cr^{VI}dm^{-3}$ paste, showing the variation in Ca (▽) and Si (●) with Cr.

After 24 h, the $CaCrO_4 \cdot 2H_2O$ crystals could not be distinguished from the regular products of hydration (Fig. 6a). The rod in the lower left corner is CH. The C–S–H fibres are shortened as the volume increase associated with the formation of fibrous C–S–H appeared inhibited. This is similar to 0.1 and 1 mol $Cr^{VI}dm^{-3}$ pastes. TEM–EDS analysis of the Cr-containing regions revealed a phase containing primarily Ca and Cr with a Ca-to-Cr ratio of 1.4 ± 0.1 (Fig. 6b).

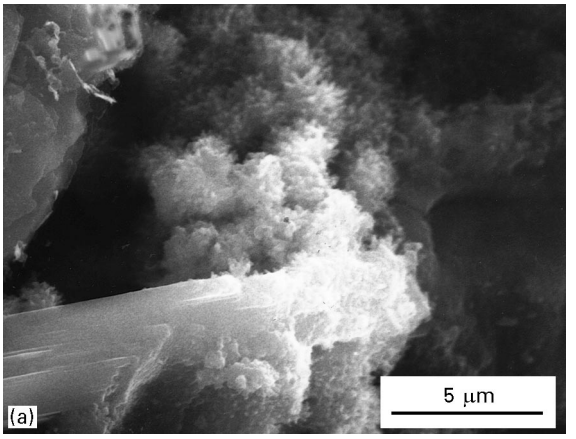

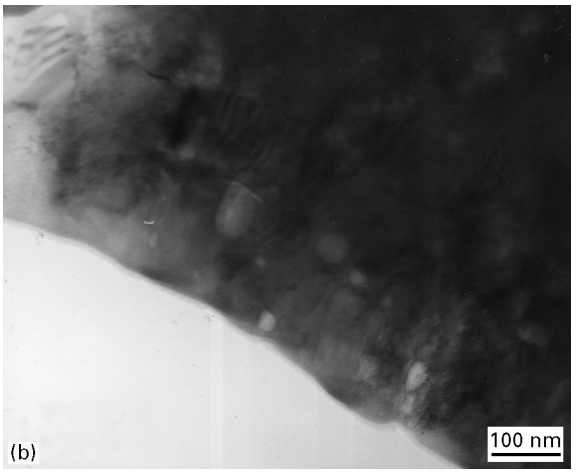

Figure 6 (a) Scanning electron micrograph of a 1-day-old 2 mol $Cr^{VI}dm^{-3}$ paste showing CH and fibrous C–S–H; (b) transmission electron micrograph of a 1-day-old 2 mol $Cr^{VI}dm^{-3}$ paste highlighting a calcium chromate phase (Ca-to-Cr ratio, about 1.38).

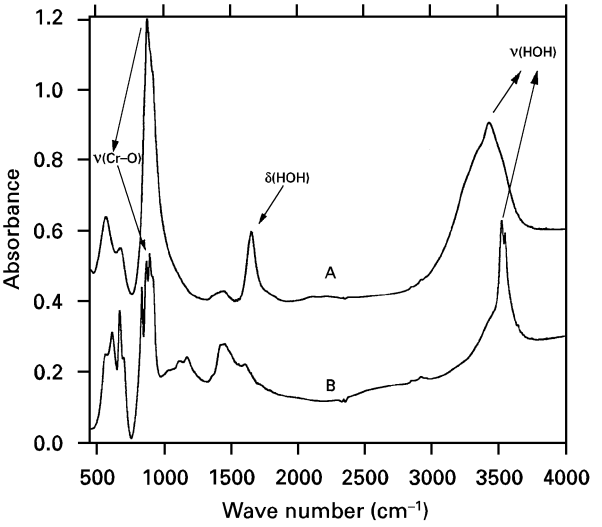

Figure 7 FTIR spectra of calcium chromates formed during hydration of Cr^{VI}-doped C_3S. Spectrum A, $CaCrO_4 \cdot 2H_2O$; spectrum B, $Ca_2CrO_5 \cdot 3H_2O$.

3.2. Infrared spectroscopy

Fig. 7 shows the infrared spectra of $CaCrO_4 \cdot 2H_2O$ and $Ca_2CrO_5 \cdot 3H_2O$, the two calcium chromates formed in Cr^{VI}-doped C_3S [46]. The spectra contain two main absorption groups: vibrational modes due to chromate ion (CrO_4^{2-}) and water of hydration.

When CrO_4^{2-} retains its tetrahedral (T_d) symmetry in a compound, four vibrational modes are present [49]. These are symmetric stretching (ν_1) at 846 cm^{-1}, in-plane bending (ν_2) at 349 cm^{-1}, asymmetric stretching (ν_3) at 890 cm^{-1} and out-of-plane bending (ν_4) at 349 cm^{-1}.

TABLE I FTIR spectra assignments for $CaCrO_4 \cdot 2H_2O$ and $Ca_2CrO_5 \cdot 3H_2O$

Spectra assignments (cm^{-1})	$CaCrO_4 \cdot 2H_2O$	$Ca_2CrO_5 \cdot 3H_2O$
*	573, 682 s, b	563, 615, 673 701 s, b
ν_1 (CrO)	–	837 sp
ν_3 (CrO)	882 s	870 s, 895 s, 916 s
*	1440 b	1112, 1168 w, b
δ (HOH)	1658 s	1637 s
ν (HOH)	3437 s, b	3528 s, 3551 s

* Unassigned bands,
s, strong; b, broad; w, weak; sp, sharp.

The presence of CrO_4^{2-} in a crystalline host may lift the degeneracies in the ν_2, ν_3 and ν_4 modes owing to distortion of the tetrahedra. ν_1 and ν_2 vibrations which are only Raman active may become infrared active, since the symmetry is lowered. A partial assignment of both spectra is shown in Table I. The strong band at 882 cm^{-1} in $CaCrO_4 \cdot 2H_2O$ was assigned to the ν_3 asymmetric stretching of the tetrahedral CrO_4^{2-} ion. There are weak shoulder bands around 882 cm^{-1} but these are unresolved in the spectra. The peaks at 682 and 573 cm^{-1} were not assigned. Sufficient distortion of the CrO_4^{2-} ion could also give dichromate-like spectra [50], with Cr–O–Cr stretching vibrations between 600 and 750 cm^{-1}. The $Ca_2CrO_5 \cdot 3H_2O$ spectrum shows a considerable split of the triply degenerate $\nu_3(CrO_4^{2-})$ asymmetric stretching vibration at 870, 895 and 916 cm^{-1}. The band at 837 cm^{-1} was assigned to the ν_1 symmetric stretch. The broad bands at 563, 615, 673 and 701 cm^{-1} are typical of dichromate spectra. However, the basic nature of $Ca_2CrO_5 \cdot 3H_2O$ (saturated solution pH, about 11) suggests the absence of dichromates in the compound. It is possible that strong Ca–O–Cr bonding exists in $Ca_2CrO_5 \cdot 3H_2O$ similar to Cr–O–Cr linkages in dichromates. In the absence of structural data on $Ca_2CrO_5 \cdot 3H_2O$, assignment of these bands is purely speculative.

In the $CaCrO_4 \cdot 2H_2O$ spectrum, the δ(HOH) bending vibration is located at 1658 cm^{-1} together with a broad ν(HOH) stretching vibration at 3437 cm^{-1}. The δ(HOH) in $Ca_2CrO_5 \cdot 3H_2O$ is at a slightly lower wave number (1637 cm^{-1}) and the ν(HOH) appeared as a doublet at 3528 and 3551 cm^{-1}.

Fig. 8 shows the infrared spectra of 2 mol $Cr^{VI}\,dm^{-3}$ pastes hydrated for 5 min, 6 h, 24 h, 72 h and 60 days. $CaCrO_4 \cdot 2H_2O$ formed within the first 5 min. The strong CrO_4^{2-} asymmetric stretch (ν_3) at 882 cm^{-1} overlaps with the SiO_4^{4-} stretching vibrations. $CaCrO_4 \cdot 2H_2O$ could not be found in any of the other spectra. Vibrational modes due to $Ca_2CrO_5 \cdot 3H_2O$ (ν(HOH) doublet at 3528 and 3551 cm^{-1}) appeared after 6 h and remained throughout the duration of the experiments. The intensities of CrO_4^{2-} and (HOH) bands remain almost constant throughout the hydration period. The ν(OH) of CH at 3644 cm^{-1} appeared in the 72 h sample and increased with age. The broad band centred at 975 cm^{-1} in the 6 h sample also intensified with age and was assigned to ν(SiOSi) asymmetric stretching vibration in C–S–H.

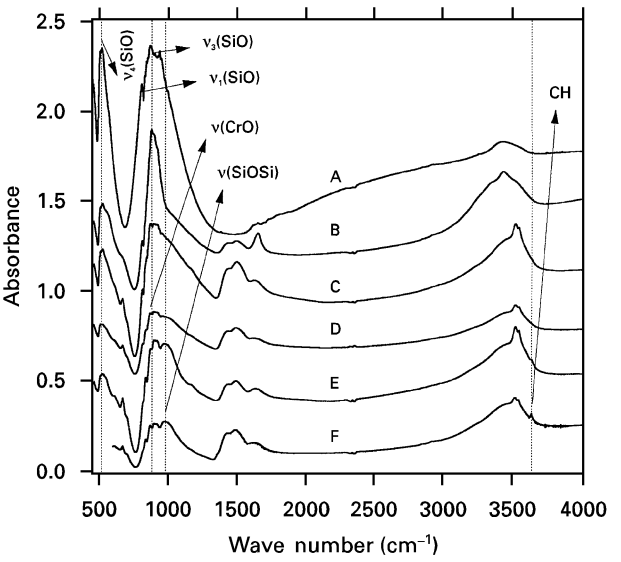

Figure 8 FTIR spectra of C_3S (spectrum A) and 2 mol $Cr^{VI}\,dm^{-3}$ pastes (spectra B–F) hydrated for 5 min, (spectrum B), 6 h, (spectrum C), 24 h, spectrum D, 72 h (spectrum E) and 60 days (spectrum F).

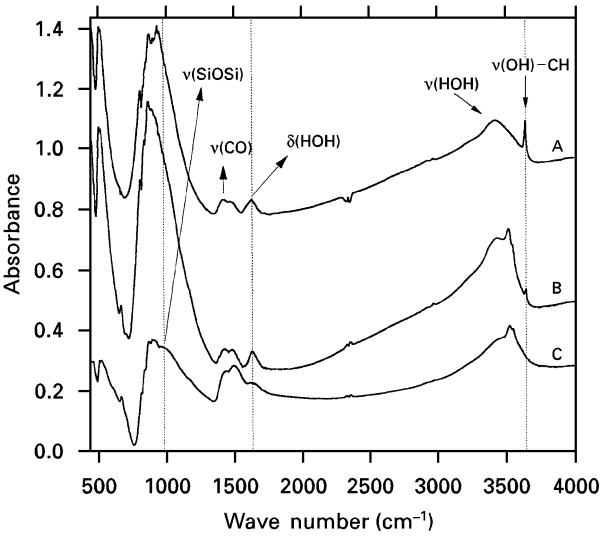

Figure 9 FTIR spectra of 24-h-old Cr^{VI} pastes. Spectrum A, blank; spectrum B; 1 mol $Cr^{VI}\,dm^{-3}$, spectrum C, 2 mol $Cr^{VI}\,dm^{-3}$.

Shown in Fig. 9 are the spectra of 1 and 2 mol $Cr^{VI}\,dm^{-3}$ pastes hydrated for 24 h. The spectrum of the blank paste was included for comparison. Apart from the $\nu(CrO_4^{2-})$ and ν(HOH) stretching vibrations, the spectrum of 1 mol $Cr^{VI}\,dm^{-3}$ paste is similar to that of the blank. The appearance of a broad Si–O–Si asymmetric stretch at 975 cm^{-1} in the 2 mol $Cr^{VI}\,dm^{-3}$ paste (not present in the standard C_3S–H_2O paste) suggests that increasing Cr^{VI} accelerated condensation of silicate units in C–S–H, during the early ages. The reduced intensity of ν(OH) of CH at 3644 cm^{-1} in the 1 mol $Cr^{VI}\,dm^{-3}$ paste and its absence in the 2 mol $Cr^{VI}\,dm^{-3}$ paste also confirms that the rate of CH formation is dependent on the concentration of the Cr^{VI} ions.

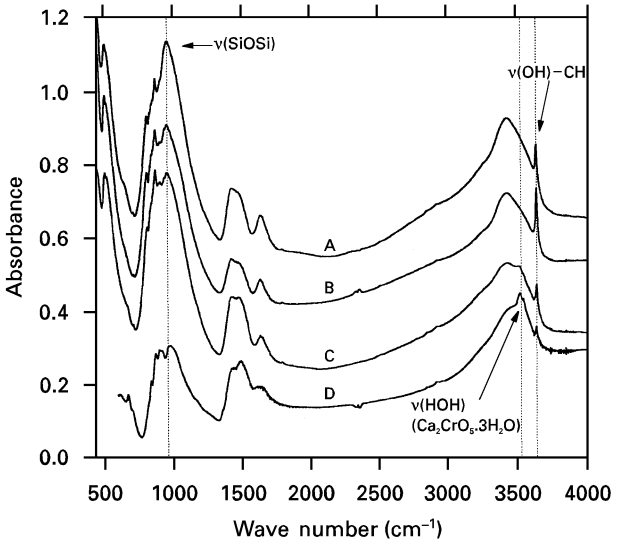

Figure 10 FTIR spectra of 60-day-old Cr^{VI} pastes: Spectrum A, blank; spectrum B, 0.1 mol $Cr^{VI}\,dm^{-3}$; Spectrum C, 1 mol $Cr^{VI}\,dm^{-3}$; spectrum D, 2 mol $Cr^{VI}\,dm^{-3}$.

In the 60-day-old 0.1 mol $Cr^{VI}\,dm^{-3}$ paste shown in Fig. 10, no $Ca_2CrO_5 \cdot 3H_2O$ vibrations were detected. The concentration of $Ca_2CrO_5 \cdot 3H_2O$ in this paste was probably too small to be detected. In the 1 and 2 mol $Cr^{VI}\,dm^{-3}$ paste the doublet ν(HOH) stretching vibrations in $Ca_2CrO_5 \cdot 3H_2O$ could still be discerned. The intensities of the CH peak at 3644 cm^{-1} also decreased with increasing concentration as was the case at 24 h. The ν(SiOSi) band at about 975 cm^{-1} becomes broader with increasing chromium concentration, suggesting that Cr^{VI} affects the structure of the C–S–H in addition to its morphology.

3.3. Nuclear magnetic resonance spectroscopy

It was found that a very long relaxation delay (up to 2 h) was necessary to obtain good signals from the pure anhydrous C_3S. In the case of hydrated pastes containing C–S–H, however, a relaxation delay of 10 s gave satisfactory signals with a good signal-to-noise ratio. Since we were primarily interested in the silicate anion structure in C–S–H, a delay time of 10 s was used in all the experiments. Because the ^{29}Si nuclei in monomeric SiO_4^{4-} in C_3S do not have sufficient time to relax, the Q_0 signals between −69 and −74 p.p.m. (representing monomeric SiO_4^{4-}) were not observed in all the spectra.

Shown in Fig. 11 are the ^{29}Si NMR spectra for 2 mol $Cr^{VI}\,dm^{-3}$ pastes. The end groups in silicate

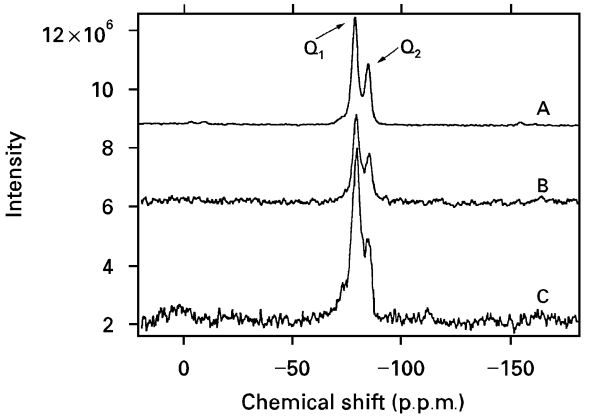

Figure 11 ^{29}Si MAS NMR spectra of partially and fully hydrated chromium-doped C_3S pastes; spectrum A, blank, 14 months; spectrum B, 2 mol $Cr^{VI}\,dm^{-3}$, 60 days; spectrum C, 2 mol $Cr^{VI}\,dm^{-3}$, 72 h.

units (Q_1) containing dimeric silicate units (Si–O–Si linkages) gave a signal at about −79 p.p.m., and middle units (Q_2) which contain polymeric silicate units, particularly pentamers and octamers, gave a signal at −85 p.p.m. These are typical of silicate units in tetrahedral coordination. The chemical shifts of octahedral silicates are usually observed to be between −200 and −250 p.p.m. [38]. None was found in any of the samples investigated. On the basis of the observed chemical shifts which are similar for the blank and Cr^{VI}, it appears that very little variation exists in the silicate anion environment in the C–S–H.

The results of trapezoidal integration of the chemical shifts are presented in Table II. This was achieved by fitting a Voigt equation to the overlapping Q_1 and Q_2 peaks. This gives a better approximation of the area than a Lorenztian fit. The rates of formation of Q_1 and Q_2 follows the established trend in normal C_3S or Portland cement hydration. Q_1 forms first and later Q_2, both forming continuously throughout the hydration reaction period. The production of Q_1 and Q_2 units proceeds at a constant rate after about 30 days [36]. After about 180 days, when most of the C_3S has reacted, the Q_2-to-Q_1 ratio obtained by several investigators is about 0.35 [1, 36]. This is similar to the Q_2-to-Q_1 ratio of 0.37 obtained in the fully hydrated blank paste used as a standard in these experiments. An interesting observation is the Q_2-to-Q_1 ratio of 60-day-old 2 mol $Cr^{VI}\,dm^{-3}$ paste (about 0.5). It is apparent that more Q_2 units are also formed than in the blank paste, reinforcing the previous conclusion from infrared analysis that condensation of the polymeric C–S–H is increased.

TABLE II ^{29}Si chemical shift data of partially and fully hydrated chromium-doped tricalcium silicate

Sample	Q_1 (ppm)		Q_2 (ppm)		Q_2-to-Q_1 integrated intensity
	Chemical shift	Linewidth	Chemical shift	Linewidth	
Blank, 14 months	−78.9	3.0	−85.0	2.6	0.37
2 mol $Cr^{VI}\,dm^{-3}$, 72 h	−79.3	4.9	−84.8	2.4	0.23
2 mol $Cr^{VI}\,dm^{-3}$, 60 days	−79.0	3.4	−85.1	3.2	0.51

Not only is the high leachability of Cr^{VI} from solidified Cr^{VI}–OPC waste form a result of the relatively high solubility of the calcium chromate phases but also the high porosity of the waste form will increase the leachant's access to chromium-containing sites within the matrix. X-ray microanalysis in the transmission electron microscope also revealed that chromium is inhomogeneously distributed in the C–S–H. No evidence of a physical mixture of amorphous C–S–H and crystalline calcium chromate was found. It is possible that some CrO_4^{2-} units are located in tetrahedral SiO_4^{4-} sites in the C–S–H. This would account for the residual Cr^{VI} observed in the leached paste after all the calcium chromates have been leached [46]. An increase in silicate condensation in the C–S–H was also observed. Even though this might not have a direct relationship on leachability, it might reduce the strength of the waste form as the fibrous (dimeric) C–S–H impacts greater strength to the matrix than the more condensed polymeric silicate units in C–S–H.

4. Conclusions

1. The fibres associated with dimeric C–S–H are much shorter, than in the blank pastes, leading to the formation of highly porous Cr^{VI} pastes.

2. Increasing Cr^{VI} concentration increases the condensation of silicates in C_3S pastes.

3. Formation of CH begins after all the chromium has been used up to form $Ca_2CrO_5 \cdot 3H_2O$.

4. The Ca-to-Si ratios of C–S–H in Cr^{VI} pastes are similar to the Ca-to-Si ratios in the blank pastes of the same age.

Acknowledgements

The authors wish to thank the Department of Natural Resources Canada (CANMET), and the Natural Sciences and Engineering Research Council of Canada for providing the financial support for this project.

References

1. H. F. W. TAYLOR, "Cement chemistry" (Academic Press, London, 1990).
2. D. L. KANTRO, *J. Test. Eval.* **3** (1975) 312.
3. I. JAWED, J. SKANLY and J. F. YOUNG, in "Structure and performance of cement," edited by P. Barnes (Applied Science, Barking, Essex 1983) p. 237.
4. N. L. THOMAS, *J. Mater. Sci.* **22** (1987) 3328.
5. O. E. OMOTOSO, D. G. IVEY and R. MIKULA, in "Treatment and minimization of heavy metal-containing wastes, edited by J.P. Hager (Minerals, Metals and Materials Society, Warrendale, PA, 1995) p. 129.
6. R. KONDO, M. DAIMON, E. SAKAI and H. J. OSHIYAMA, *J. Appl. Chem. Biotechnol.* **27** (1977) 191.
7. H. G. MIDGLEY, *Cem. Concr. Res.* **9** (1979) 77.
8. I. ODLER and H. DORR, *ibid.* **9** (1979) 239.
9. A. BENTUR and R. L. BERGER, *J. Amer. Ceram. Soc.* **62** (1979) 117.
10. V. S. RAMACHANDRA, *Cem. Concr. Res.* **9** (1979) 677.
11. R. B. WILLIAMSON, *Prog. Mater. Sci.* **15** (1972) 189.
12. S. DIAMOND, in "Proceedings of the Conference on Hydraulic Cement Pastes; Their Structure and Properties," (Cement and Concrete Association, London, 1976) p. 2.
13. S. GOTO, M. DAIMON, G. HOSAKA and R. KONDO, *J. Amer. Ceram. Soc.* **59** (1976) 281.
14. B. MARCHESE, *Cem. Concr. Res.* **7** (1977) 9.
15. *Idem. J. Amer. Ceram. Soc.* **61** (1978) 349.
16. G. W. GROVES, *Mater. Res. Soc. Symp. Proc.* **85** (1987) 3.
17. M. S. STUCKE and A. J. MAJUMDAR, *Cem. Concr. Res.* **7** (1977) 711.
18. K. L. SCRIVENER, H. H. PATEL, P. C. PRATT and C. J. PARROT, *Mater. Res. Soc. Symp. Proc.* **85** (1987) 67.
19. A. GRUDEMO, in "The chemistry of cement," Part I, edited by H.F.W. Taylor (Academic Press, London, 1964) p. 371.
20. D. D. DOUBLE, *Mater. Sci. Engng* **12** (1973) 29.
21. F. W. LAWRENCE Jr and A. A. DE CARVALHO, *J. Amer. Ceram. Soc.* **57** (1974) 144.
22. B. J. DALGLEISH and K. IBE, *Cem. Concr. Res.* **11** (1981) 729.
23. H. M. JENNINGS, B. J. DALGLEISH and P. L. PRATT, *J. Amer. Ceram. Soc.* **64** (1981) 567.
24. S. A. RODGER, G. W. GROVES, N. J. CLAYDEN and C. M. DOBSON, *Mater. Res. Soc. Symp. Proc.* **85** (1987) 13.
25. D. G. IVEY and M. NEUWIRTH, *Cem. Concr. Res.* **19** (1989) 642.
26. H. F. W. TAYLOR and D. E. NEWBURY, *ibid.* **14** (1984) 93.
27. J. A. GARD, K. MOHAN, H. F. W. TAYLOR and G. CLIFF, *J. Amer. Ceram. Soc.* **63** (1981) 336.
28. K. MOHAN and H. F. W. TAYLOR, *ibid.* **64** (1981) 717.
29. A. N. LAZAREV, "Vibrational spectra and structure of silicates" (Consultant Bureau, New York, 1972).
30. F. LIBEAU, "Structural chemistry of silicates" (Springer, Berlin, 1985).
31. F. MATOSSI, *J. Chem. Phys.* **17** (1949) 679.
32. J. ETCHEPARE, *Spectrochim. Acta A* **26** (1970) 2147.
33. M. HANDKE, *Appl. Spectrosc.* **40** (1986) 871.
34. E. LIPPMAA, M. MAGI, A. SAMSON, G. ENGELHARRDT and A. R. GRIMMER, *J. Amer. Chem. Soc.* **102** (1980) 4889.
35. E. LIPPMAA, M. MAGI, M. TARMAK, W. WIEKER and A. R. GRIMMER, *Cem. Concr. Res.* **12** (1982) 597.
36. N. J. CLAYDEN, C. M. DOBSON, G. W. GROVES, C. J. HAYES and S. A. RODGER, *Brit. Ceram. Soc. Proc.* **35** (1984) 55.
37. J. R. BARNES, A. D. H. CLAGUE, N. J. CLAYDEN, C. M. DOBSON, C. J. HAYES, G. W. GROVES and S. A. RODGER, *J. Mater. Sci. Lett.* **4** (1985) 1293.
38. A. R. GRIMMER and F. VON LAMPE, *Chem. Phys. Lett.* **132** (1986) 549.
39. J. HJORTH, J. SKIBSTED and H. J. JAKOBSEN, *Cem. Concr. Res.* **18** (1988) 789.
40. S. A. RODGER, G. W. GROVES, N. J. CLAYDEN and C. M. DOBSON, *J. Amer. Ceram. Soc.* **71** (1988) 91.
41. G. PARRY-JONES, A. J. AL - TAYYIB and A. I. AL-MANA, *Cem. Concr. Res.* **18** (1988) 229.
42. *Idem., ibid.* **19** (1989) 228.
43. H. ISHIDA, Y. OKADA and T. MITSUDA, *J. Amer. Ceram. Soc.* **75** (1992) 359.
44. F. K. CARTELEDGE, Private communication.
45. J. D. ORTEGO, Y. BARROETA, F. K. CARTLEDGE and H. AKHTER, *Environ. Sci. Technol.* **25** (1991) 1171.
46. O. E. OMOTOSO, D. G. IVEY and R. J. MIKULA, *J. Mater. Sci.* **33** (1998) 507.
47. D. H. CAMPBELL and W. U. AHMED, *Microstruct. Sci.* **7** (1979) 369.
48. D. G. IVEY, R. J. MIKULA, W. W. LAM, M. NEUWIRTH, D. J. CONRAD and R. B. HEIMANN, in "Proceedings of the Symposium on Cement Industry Solutions to Waste Management" (Canadian Portland Cement Association, Calgary, 1992).
49. K. NAKAMOTO, "Infrared and Raman spectra of inorganic and coordination compounds" (Wiley, New York, 4th Edn, 1986).
50. J. A. GADSDEN, "Infrared spectra of minerals and related inorganic compounds" (Butterworth, London, 1975).

Received 19 April
and accepted 19 December 1996